Radiation Protection Dosimetry (2020), Vol. 189, No. 2, pp. 163–171 doi:10.1093/rpd/ncaa027
Advance Access publication 14 April 2020

INVESTIGATION OF THE INFLUENCE OF THYROID LOCATION ON IODINE-131 S VALUES

Yeon Soo Yeom[1,*], Daphnée Villoing[1], Natasha Greenstein[2], Cari M. Kitahara[1], Les R. Folio[3], Chan Hyeong Kim[4], and Choonsik Lee[1]
[1]Division of Cancer Epidemiology and Genetics, National Cancer Institute, National Institutes of Health, Rockville MD 20850, USA
[2]Bethesda-Chevy Chase High School, Bethesda, MD 20852, USA
[3]Radiology and Imaging Sciences, Clinical Center, National Institutes of Health, Bethesda, MD 20852, USA
[4]Department of Nuclear Engineering, Hanyang University, Seoul, Korea

*Corresponding author: yeonsoo.yeom@nih.gov

Received 8 November 2019; revised 19 January 2020; editorial decision 11 February 2020; accepted 11 February 2020

The use of iodine-131 S values based on reference computational phantoms with fixed thyroid model may lead to significant dosimetric errors in patients who may have different thyroid location from the reference phantoms. In the present study, we investigated individual thyroid location variation by examining the computed tomography image sets of 40 adult male and female patients. Subsequently, the thyroid location of the adult male and female mesh-type reference phantoms of the International Commission on Radiological Protection (ICRP) was adjusted to match each the highest, mean and the lowest locations of the thyroid observed in this dataset. The thyroid-adjusted phantoms were implemented into the Geant4 Monte Carlo code to calculate thyroid location-dependent iodine-131 S values ($r_T \leftarrow$ thyroid) for a total of 30 target regions. The maximum variation among the observed thyroid locations was 39 mm and 36 mm for male and female patients, respectively. The mean thyroid locations of both male and female patients showed a good agreement with the ICRP reference phantoms. The thyroid location-dependent Iodine-131 S values were significantly different from the reference phantoms for most target regions by up to a factor of 3. The use of thyroid location-dependent S values in dose reconstructions should help quantify the dosimetric uncertainty in epidemiologic investigations of patients receiving iodine-131 therapy for hyperthyroidism and thyroid cancer.

INTRODUCTION

Since the mid-20th century, radioactive iodine (RAI) has been extensively used for the treatment of hyperthyroidism and thyroid cancer[1, 2]. During the course of the treatment, iodine-131 is predominantly retained in the thyroid[3]. However, exposure to other organs and tissues from emitted beta and gamma radiations is unavoidable, and late health effects to normal organs and tissues after RAI treatment are of concern. Assessment of the risks of radiation-induced cancer and other late effects among RAI-treated patients relies on accurate estimation of radiation dose to radiosensitive organs and tissues[4, 5].

To estimate organ/tissue absorbed doses for a cohort of patients with hyperthyroidism treated with RAI[6], Lamart *et al.*[7] established a comprehensive dataset of iodine-131 dose conversion coefficients, called S values ($r_T \leftarrow r_S$) [mGy (Bq s)$^{-1}$]: the mean absorbed doses delivered to target tissues per unit disintegration of the radionuclide in source regions[8]. The S values were calculated by conducting Monte Carlo radiation transport simulations with the adult male and female voxel-type reference computational phantoms of International Commission on Radiological Protection (ICRP) described in ICRP Publication 110[9]. The use of these S values based on the ICRP reference voxel phantoms constructed from computed tomography (CT) patient images may have improved the accuracy of dose estimates when compared to the previous values based on stylized phantoms represented by mathematical equations[10]. However, the new S values were based on the reference phantoms with fixed anatomy. Uncertainties that may be caused by possible variation in the thyroid location have not yet been quantified.

To fill this critical gap, in the present study, we investigated individual variation of thyroid location by examining 40 sets of neck CT images of adult male and female patients. Then, the mesh-type ICRP reference computational phantoms (MRCPs) for adult male and female[11, 12], the mesh-format counterparts of the ICRP reference voxel phantoms, were modified to move the thyroid into the highest, mean and the lowest locations observed from the patient CT data. The modified phantoms were implemented into the Geant4 Monte Carlo code[13] to calculate thyroid location-dependent S values for iodine-131 and for 30 radiosensitive target organs/tissues. The calculated S values dependent on thyroid locations were compared with those calculated with the MRCPs with the fixed thyroid location to investigate the impact of individual variation of thyroid location on the S values.

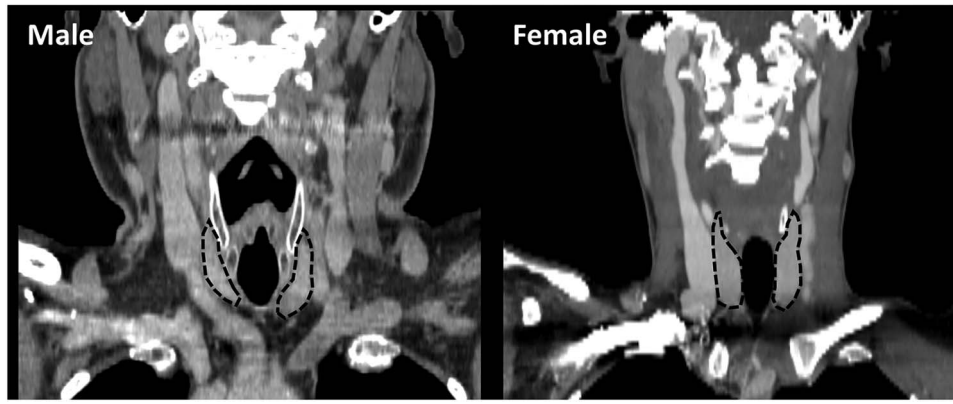

Figure 1. Coronal views of the neck CT scans for adult male (left) and female (right) patients with the thyroid contours marked by dashed lines. This comparison demonstrates a generalized example of anatomic variability of the thyroid.

MATERIALS AND METHODS

Measurement of thyroid location

A total of 40 neck CT image sets of 20 adult male and 20 adult female patients were randomly selected from the CT image archive at the National Institutes of Health Clinical Center, which was part of the Institutional Review Board exempt study. The 40 patients were on average 52 years old (20–76 years). All scans were conducted on any of Siemens Definition, Flash or Force using the similar protocol with the tube potential of 120 kVp.

We adopted a CT image processing software, ImageJ (https://imagej.nih.gov/ij/), to measure the thyroid location. Distance between the top of the first cervical vertebrae (C1) and the top of the thyroid was measured by counting the number of CT slices in-between multiplied by the Z resolution. When the left and right tops of the thyroid are asymmetric, an average was used. During the measurement, we excluded four CT image sets (three males and one female) in which the thyroid was not able to be identified due to the poor contrast. The CT images and the measurements were reviewed by a radiologist. Figure 1 shows the coronal views of two example CT image sets for an adult male and female with the thyroid contours marked in red solid lines.

Mesh-type ICRP reference computational phantoms

To simulate the individual variation of the thyroid location within the human anatomy, we employed the adult male and female MRCPs. These MRCPs are the new ICRP reference phantoms constructed by converting the voxel-type ICRP reference phantoms[9] into high-quality/fidelity polygonal mesh (PM) or tetrahedral mesh (TM)[11]. The MRCPs maintain the anatomy of the ICRP reference voxel phantoms, while overcoming the limitations of the voxel phantoms due to the limited voxel resolutions and the nature of voxel geometry. Especially, the mesh geometry of the MRCPs has higher deformability/flexibility than the voxel geometry of the ICRP voxel phantoms, which allowed us to adjust the location of the thyroid in the current study.

The thyroids of the MRCPs were moved to the three locations (the highest, mean and the lowest), which were measured from the CT image sets. We imported the MRCPs in the PM format into a mesh modeling software, *Geomagic Design X* (3D Systems, Rock Hill, SC, USA). The thyroid of the phantoms was moved in z direction to the target locations by using the *Transform Scan Data* tool of the software. Overlaps between the thyroid at the new locations and surrounding organs/tissues were eliminated by adjusting the neighbor organs/tissues through refinement tools (*Healing Wizard, Smart Bruch and Fill Holes*), while maintaining their original volumes (i.e. masses). The modified phantoms in the PM format were finally converted to the TM format through a tetrahedralization process by using the TetGen code[14]. A total of six phantoms were created: three males and three females with the highest, mean and the lowest thyroid locations.

Calculation of S values for ^{131}I

Monte Carlo particle transport simulations were conducted to calculate S values ($r_T \leftarrow$ thyroid) for ^{131}I of the modified phantoms as well as the original MRCPs for the 30 radiosensitive target organs/tissues[15]: red bone marrow (RBM), colon, lung, stomach, breast, testis, ovaries, urinary bladder, esophagus, liver, thyroid, endosteum, brain, salivary glands, skin, adrenals, extrathoracic (ET) region, gall bladder, heart, kidneys, lymph nodes, muscle, oral

mucosa, pancreas, prostate, uterus, small intestine, spleen, thymus and eye lens.

The phantoms in TM format were implemented into the Geant4 Monte Carlo code[13] via the *G4Tet* class following the implementation procedure previously published by Yeom *et al.*[16]. Beta and gamma radiations emitted from the thyroid, in which ^{131}I was assumed to be uniformly distributed, were simulated by using the *G4UserPrimaryGeneratorAction* class. The energy spectra of the emitted radiations were obtained from the nuclear decay data produced in ICRP Publication 107[17]. To transport electrons and photons, the electromagnetic physics library of *G4EmLivermorePhysics* was applied with a secondary production cut value of 1 μm. Absorbed doses for all the organs/tissues, with exceptions of the skeletal tissues (i.e. RBM and endosteum), were directly calculated from the phantoms by using the *G4PSEnergyDeposit* class. Note that the microscopic structures of the RBM and endosteum were not explicitly represented in the spongiosa and medullary cavities of the MRCPs[18] as well as the modified phantoms. The skeletal absorbed doses for betas were estimated as the mass-weighted average of the regional spongiosa and medullary cavity doses following the approach described in ICRP Publication 116[19], while those for gammas were estimated by using the fluence-to-absorbed dose response functions reported by Johnson *et al.*[20]. A total of 10^{10} primary particles for each calculation were transported so that the statistical relative errors for the calculated absorbed doses (i.e. S values) for all target organs/tissues were <5%. The simulations were conducted on Biowulf, the National Institutes of Health's high-performance Linux computing cluster (https://hpc.nih.gov). We first compared the S values calculated from the original MRCPs with the values previously published by Lamart *et al.*[7] using the ICRP voxel phantoms to make sure the two values agree. Then we evaluated the impact of the thyroid location on S values.

RESULTS AND DISCUSSION

Variation of thyroid location

Figure 2 shows the distances between the tops of the C1 vertebrae and thyroid for 17 adult males and 19 adult females. The distances for males show a range from 76 to 115 mm, whereas those for females show a range from 68 to 104 mm. The mean distances for males and females are 97 and 85 mm, respectively, which are comparable with those of the MRCPs (male: 104 mm and female: 88 mm). The difference between the highest and the lowest locations was 39 and 36 mm for males and females, respectively. The C1-to-thyroid distances for males tend to be longer than those for females; this tendency is statistically significant according to the two-sample *t*-test ($P = 0.001$).

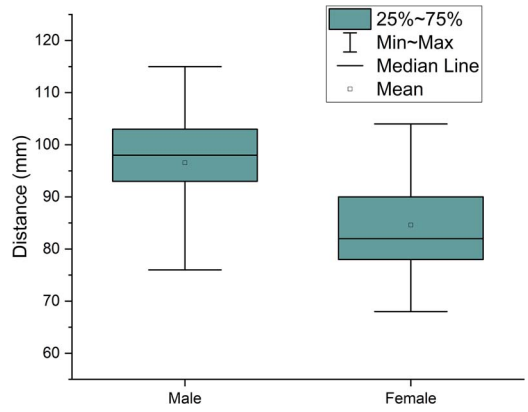

Figure 2. Distribution of the distances between the C1 vertebrae and thyroid measured for 17 male and 19 female patients.

Comparison between mesh-type and voxel-type ICRP reference phantoms

Figure 3 shows the ratios of the S values from the original MRCPs to the values from the ICRP voxel phantoms. The ratios for most organs/tissues are close to unity (between 0.9 and 1.1), which confirms that the MRCPs generally provide the similar S values to the ICRP voxel phantoms despite the different geometry formats: mesh vs. voxel. Meanwhile, notably large differences between the two phantom types can be observed in the lymph nodes, the ratios of which are 0.13 and 0.20 for male and female, respectively. These differences can be explained by the improved representation of the lymph nodes in the MRCPs over the ICRP voxel phantoms. The lymph nodes of the ICRP voxel phantoms, which could not be identified on the original CT images, were manually drawn[9] and do not represent the site-specific counts of the lymph nodes presented in ICRP Publication 89[21]. To address the limitation, the lymph nodes of the MRCPs were generated by using an advanced modeling approach previously published[22] based on the site-specific lymph node data derived from the data of ICRP Publications 23, 66, and 89[21, 23, 24].

Modified phantoms in different thyroid locations

Figure 4 shows the original MRCPs (first column) along with the modified phantoms (next three columns), showing how the thyroid locations of the phantoms are different. Note that the body height and weight and masses of all organs/tissues of the

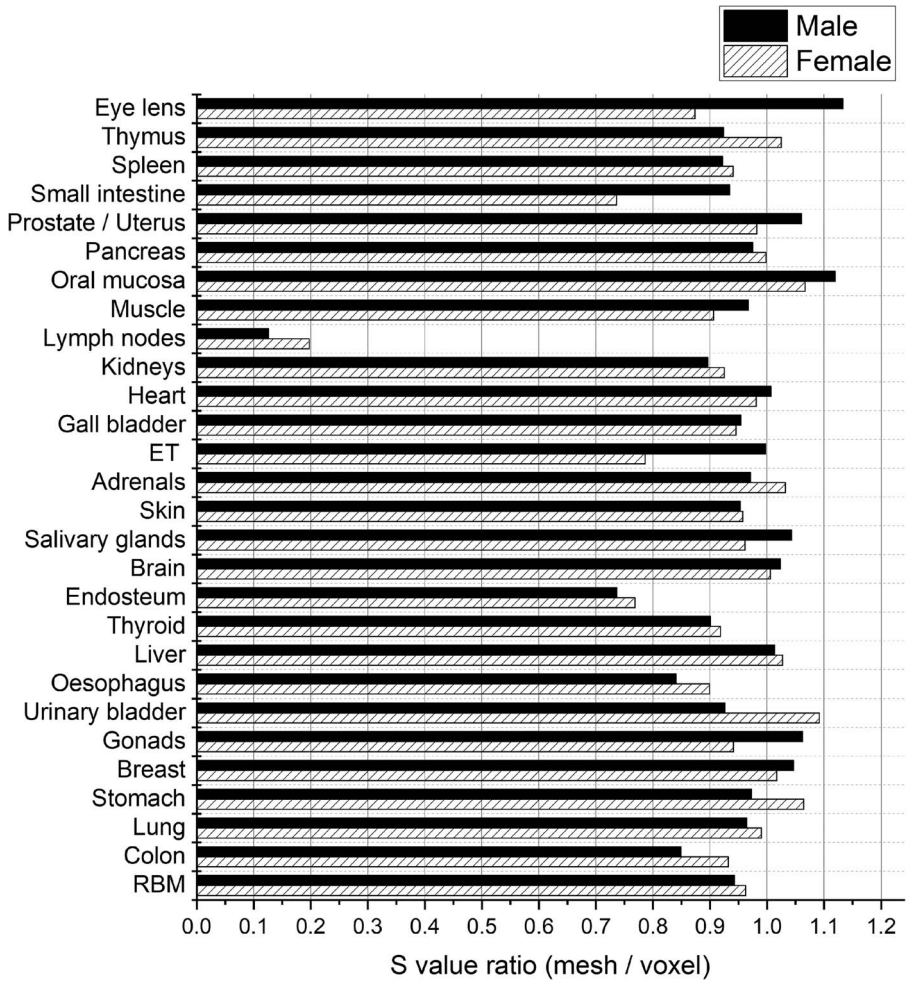

Figure 3. Ratios of S values of the mesh-type ICRP reference phantoms calculated in the present study with respect to the values of the voxel-type ICRP reference phantoms calculated in Lamart *et al.*[7].

modified phantoms are identical to those of the MRCPs.

S values dependent on thyroid location

Tables 1 and 2 show the S values ($r_T \leftarrow$ thyroid) for ^{131}I calculated from the three modified phantoms in the different thyroid locations (i.e. the highest, mean and the lowest) and the original MRCPs.

Figures 5 and 6 show the ratios of the S values of the modified phantoms to the values from the original MRCPs for male and female, respectively. The ratios for the mean thyroid locations are generally close to unity (mostly between 0.9 and 1.1), which means the original MRCPs provide representative S values for the patients with mean thyroid locations. This can be explained by the observation in Section Variation of thyroid location: the thyroid locations of the MRCPs are similar to the mean thyroid locations. The largest difference is observed in the male thymus where the S value of the MRCP is 27% greater than that of the modified phantom.

For the highest thyroid locations, the ratios for most organs/tissues are smaller than unity; that is, the MRCPs overestimate the S values of the patients with higher thyroid locations than the mean location. The largest difference for both genders is observed in the thymus, in which the S values of the MRCPs are 3.2 (male) and 2.4 (female) times greater than those from the phantoms with the highest thyroid locations. The difference can be explained by the shorter distances of these organs/tissues from the thyroid compared to

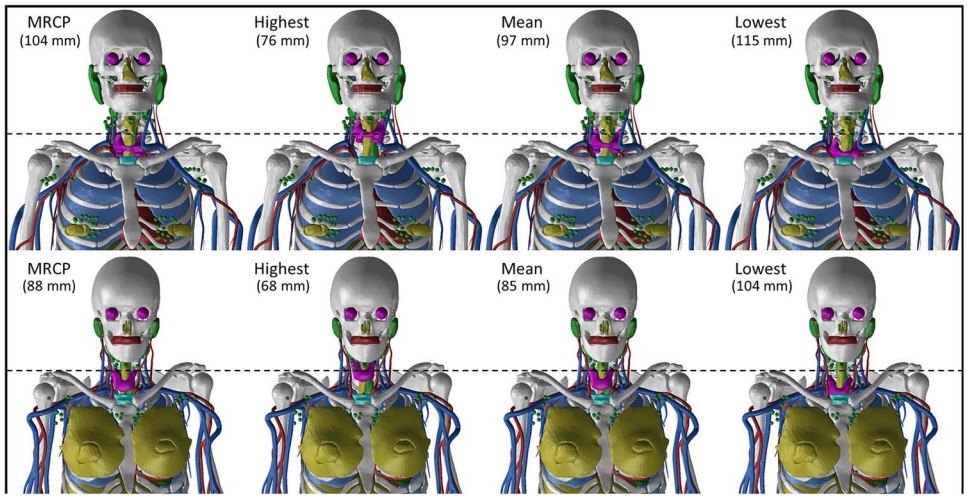

Figure 4. MRCPs (first column) along with the three phantoms (next three columns) with three different thyroid locations (the highest, mean and the lowest) for male (top row) and female (bottom row). Dotted lines were drawn at the top level of the thyroids in MRCPs to help comparing the thyroid levels of other three modified phantoms.

Table 1. S values ($r_T \leftarrow$ thyroid) for ^{131}I [mGy (Bq s)$^{-1}$] for the original MRCP and the three modified phantoms in different thyroid locations for adult male.

Target organs/tissues	MRCP	Thyroid locations of modified phantoms		
		Highest	Mean	Lowest
RBM	5.46E-13	3.72E-13	5.36E-13	6.04E-13
Colon	2.79E-14	1.99E-14	2.60E-14	3.27E-14
Lung	8.81E-13	4.56E-13	7.78E-13	1.12E-12
Stomach	1.15E-13	7.80E-14	1.05E-13	1.35E-13
Breast	1.41E-13	1.40E-13	1.17E-13	1.60E-13
Testis	3.34E-16	2.88E-16	3.12E-16	3.89E-16
Urinary bladder	2.53E-15	1.82E-15	2.41E-15	3.18E-15
Esophagus	6.29E-12	3.46E-12	6.44E-12	6.90E-12
Liver	1.46E-13	9.32E-14	1.33E-13	1.71E-13
Thyroid	1.43E-09	1.43E-09	1.43E-09	1.43E-09
Endosteum	2.45E-13	2.00E-13	2.50E-13	2.57E-13
Brain	1.56E-13	2.39E-13	1.75E-13	1.31E-13
Salivary glands	9.59E-13	2.27E-12	1.14E-12	7.37E-13
Skin	1.33E-13	1.82E-13	1.36E-13	1.25E-13
Adrenals	9.43E-14	5.92E-14	8.82E-14	1.10E-13
ET region	1.92E-12	6.34E-12	2.38E-12	1.27E-12
Gall bladder	8.10E-14	5.43E-14	7.41E-14	9.39E-14
Heart	6.51E-13	3.46E-13	5.68E-13	8.32E-13
Kidneys	5.23E-14	3.34E-14	4.84E-14	6.04E-14
Lymph nodes	2.90E-13	4.02E-13	3.23E-13	2.62E-13
Muscle	2.38E-13	2.19E-13	2.49E-13	2.35E-13
Oral mucosa	8.14E-13	1.74E-12	9.60E-13	6.59E-13
Pancreas	6.95E-14	4.61E-14	6.32E-14	8.12E-14
Prostate	1.45E-15	1.06E-15	1.27E-15	1.61E-15
Small intestine	2.23E-14	1.46E-14	2.03E-14	2.68E-14
Spleen	1.44E-13	9.01E-14	1.34E-13	1.66E-13
Thymus	7.82E-12	2.46E-12	5.70E-12	1.24E-11
Eye lens	1.52E-13	2.69E-13	1.64E-13	1.14E-13

Table 2. S values ($r_T \leftarrow$ thyroid) for ^{131}I [mGy (Bq s)$^{-1}$] for the original MRCP and the three modified phantoms in different thyroid locations and for adult female.

Target organs/tissues	MRCP	Thyroid locations of modified phantoms		
		Highest	Mean	Lowest
RBM	6.52E-13	5.82E-13	6.50E-13	7.75E-13
Colon	1.08E-14	8.12E-15	1.03E-14	1.37E-14
Lung	9.88E-13	6.55E-13	9.39E-13	1.46E-12
Stomach	9.18E-14	6.66E-14	9.37E-14	1.12E-13
Breast	3.19E-13	2.66E-13	3.05E-13	4.06E-13
Ovaries	2.32E-15	1.68E-15	2.30E-15	3.00E-15
Urinary bladder	2.47E-15	1.73E-15	2.40E-15	2.84E-15
Esophagus	7.84E-12	6.70E-12	8.00E-12	7.90E-12
Liver	1.50E-13	1.11E-13	1.44E-13	1.96E-13
Thyroid	1.72E-09	1.72E-09	1.72E-09	1.72E-09
Endosteum	3.17E-13	3.25E-13	3.22E-13	3.38E-13
Brain	2.51E-13	3.65E-13	2.66E-13	1.89E-13
Salivary glands	1.63E-12	3.16E-12	1.78E-12	1.05E-12
Skin	1.77E-13	1.91E-13	1.78E-13	1.57E-13
Adrenals	9.44E-14	7.09E-14	9.02E-14	1.23E-13
ET region	2.30E-12	5.66E-12	2.64E-12	1.32E-12
Gall bladder	8.65E-14	6.73E-14	8.23E-14	1.09E-13
Heart	6.63E-13	4.42E-13	6.26E-13	9.40E-13
Kidneys	4.93E-14	3.75E-14	4.77E-14	6.31E-14
Lymph nodes	4.44E-13	6.78E-13	4.53E-13	3.90E-13
Muscle	3.23E-13	3.26E-13	3.23E-13	3.06E-13
Oral mucosa	1.83E-12	3.45E-12	1.99E-12	1.15E-12
Pancreas	5.44E-14	4.15E-14	5.20E-14	6.83E-14
Uterus	2.20E-15	1.73E-15	2.04E-15	2.70E-15
Small intestine	1.44E-14	1.18E-14	1.37E-14	1.92E-14
Spleen	1.15E-13	8.98E-14	1.11E-13	1.42E-13
Thymus	7.86E-12	3.24E-12	6.67E-12	1.69E-11
Eye lens	2.27E-13	3.12E-13	2.12E-13	1.69E-13

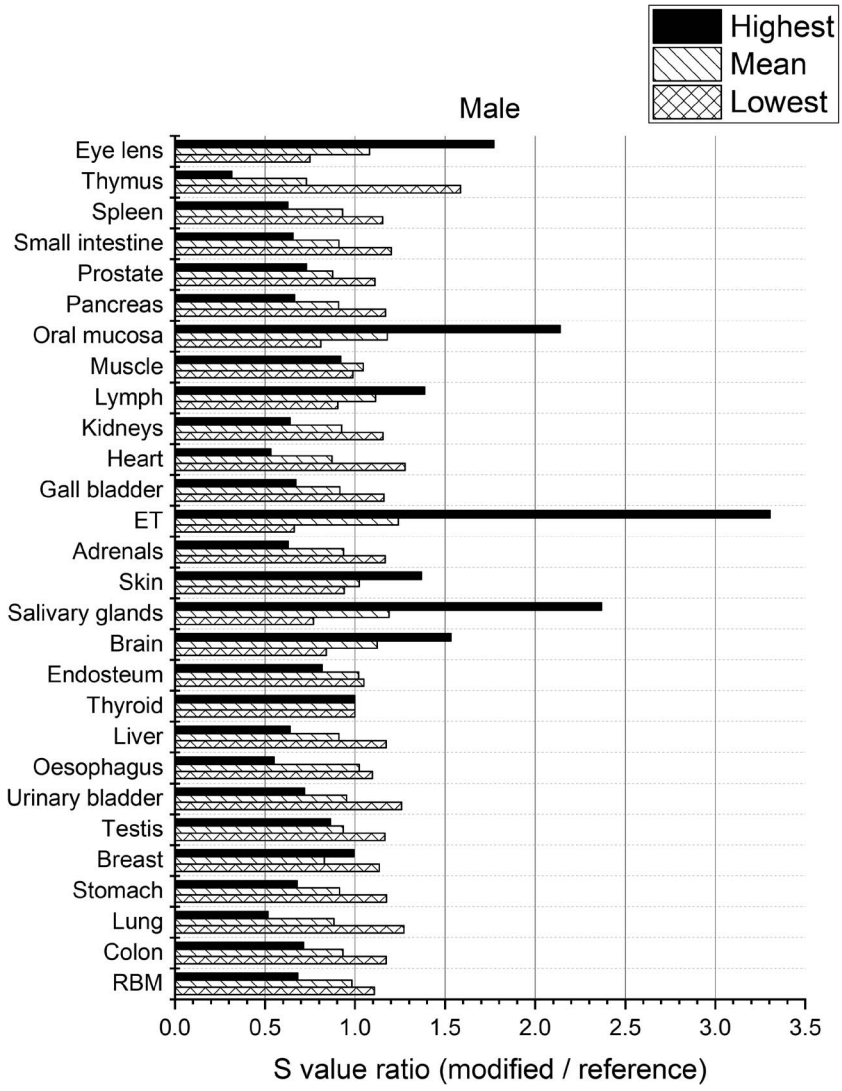

Figure 5. Ratios of S values of the male modified phantoms in the highest, mean and the lowest thyroid locations with respect to the values from the male mesh-type ICRP reference phantom.

the modified phantoms in the highest thyroid locations, resulting that the radiations emitted from the thyroid were less attenuated in the MRCPs before reaching the target organs/tissues. On the other hand, some organs/tissues such as ET and brain show the ratios are greater than unity; that is, the S values of the MRCPs are lower than those of the modified phantoms. The largest difference for both genders is observed in the ET, in which the S values of the MRCPs are lower by a factor of 3.3 and 2.5 for male and female, respectively. This can be explained by the fact that the organs/tissues, mostly located in the head and neck region, have longer distances from the thyroid compared to the modified phantoms in the highest thyroid locations.

The trend of the S value differences from the MRCPs for the highest thyroid locations is reversed in that for the lowest thyroid locations. That is, the ratios for most organs/tissues are greater than unity; the S values of the MRCPs are lower than those of the modified phantoms in the lowest thyroid locations. The largest difference for both genders is observed again in the thymus, in which the S values of the MRCPs are lower by a factor of 1.6 and 2.2 for male and

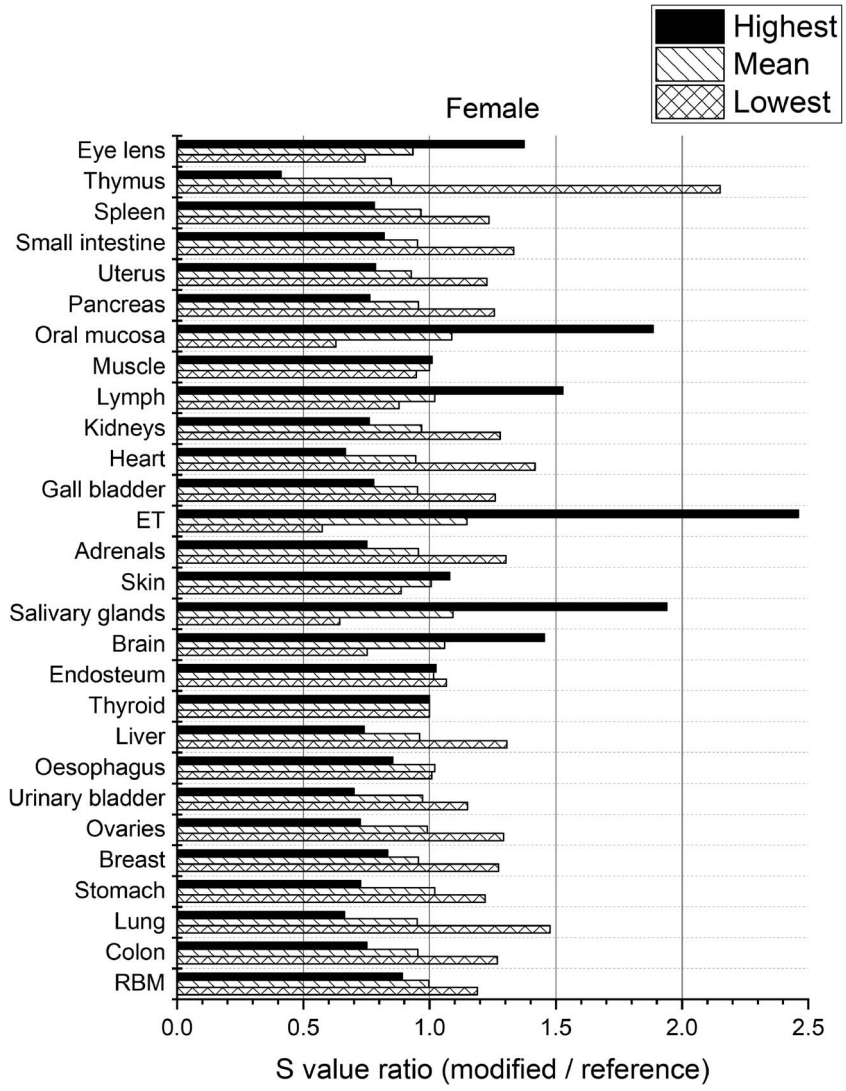

Figure 6. Ratios of S values of the female modified phantoms in the highest, mean and the lowest thyroid locations with respect to the values from the female mesh-type ICRP reference phantom.

female, respectively. Meanwhile, some organs/tissues mostly in the head and neck region show the ratios are smaller than unity; the S values of the MRCPs are greater than those of the modified phantoms. The largest difference for both genders is observed again in the ET, in which the S values of the MRCPs are greater by a factor of 1.5 and 1.7 for male and female, respectively.

CONCLUSION

We investigated the impact of different thyroid locations on internal dose conversion coefficients, S values, by calculating these values using the computational human phantoms with different thyroid locations measured from adult neck CT images. The mean thyroid locations were observed in a good agreement

with those of the adult MRCPs. However, we found that there is indeed significant individual variation in the thyroid location, which provides up to 3-fold difference in S values from the thyroid to many target organs and tissues. We believe that the S values dependent on the thyroid location should be helpful to improve dose reconstructions of patients internally exposed to ^{131}I for risk assessment in epidemiologic investigations by taking the patient thyroid location variation into account.

ACKNOWLEDGEMENT

This research was funded by the intramural research program of the National Institutes of Health (NIH), National Cancer Institute, Division of Cancer Epidemiology and Genetics. One of the authors (Yeon Soo Yeom) was supported by a grant of the Korean Health Technology R&D Project through the Korean Health Industry Development Institute (KHIDI) funded by the Ministry of Health & Welfare, Republic of Korea (Project No.: H18C2257). The calculations in this work were performed on the NIH's High-Performance Computing Biowulf cluster (https://hpc.nih.gov).

REFERENCES

1. Beierwaltes, W. H., Rabbani, R., Dmuchowski, C., Lloyd, R. V., Eyre, P. and Mallette, S. *An analysis of "ablation of thyroid remnants" with I-131 in 511 patients from 1947-1984: experience at University of Michigan*. J. Nucl. Med. **25**, 1287–1293 (1984).
2. Meier, D. A., Brill, D. R., Becker, D. V., Clarke, S. E. M., Silberstein, E. B., Royal, H. D. and Balon, H. R. *Procedure guideline for therapy of thyroid disease with ^{131}I odine*. J. Nucl. Med. **43**, 856–861 (2002).
3. Ron, E. *et al. Cancer mortality following treatment for adult hyperthyroidism. Cooperative thyrotoxicosis therapy follow-up study group*. JAMA **280**, 347–355 (1998).
4. Smith, T. and Edmonds, C. J. *Radiation dosimetry in the treatment of thyroid carcinoma by ^{131}I*. Radiat. Prot. Dosim. **5**, 141–149 (1983).
5. Willegaignon, J., Stabin, M. G., Guimarães, M. I. C., Malvestiti, L. F., Sapienza, M. T., Maroni, M. and Sordi, G.-M. A. A. *Evaluation of the potential absorbed doses from patients based on whole-body ^{131}I clearance in thyroid cancer therapy*. Health Phys. **91**, 123–127 (2006).
6. Melo, D. R., Brill, A. B., Zanzonico, P., Vicini, P., Moroz, B., Kwon, D., Lamart, S., Brenner, A., Bouville, A. and Simon, S. L. *Organ dose estimates for hyperthyroid patients treated with ^{131}I: an update of the thyrotoxicosis follow-up study*. Radiat. Res. **184**, 595–610 (2015).
7. Lamart, S., Simon, S. L., Bouville, A., Moroz, B. E. and Lee, C. *S values for ^{131}I based on the ICRP adult voxel phantoms*. Radiat. Prot. Dosim. **168**, 92–110 (2016).
8. Bolch, W. E., Eckerman, K. F., Sgouros, G. and Thomas, S. R. *MIRD pamphlet no. 21: A generalized schema for radiopharmaceutical Dosimetry—Standardization of nomenclature*. J. Nucl. Med. **50**, 477–484 (2009).
9. ICRP. *Adult reference computational phantoms*. Ann. ICRP, ICRP Publication 110 **39**, 1–166 (2009).
10. Lamart, S., Bouville, A., Simon, S. L., Eckerman, K. F., Melo, D. and Lee, C. *Comparison of internal dosimetry factors for three classes of adult computational phantoms with emphasis on I-131 in the thyroid*. Phys. Med. Biol. **56**, 7317–7335 (2011).
11. Kim, C. H. *et al. New mesh-type phantoms and their dosimetric applications, including emergencies*. Ann. ICRP **47**, 45–62 (2018).
12. Yeom, Y. S., Han, M. C., Kim, C. H. and Jeong, J. H. *Conversion of ICRP male reference phantom to polygon-surface phantom*. Phys. Med. Biol. **58**, 6985 (2013).
13. Allison, J. *et al. Recent developments in Geant4*. Nucl. Instrum. Methods Phys. Res., Sect. A **835**, 186–225 (2016).
14. Si, H. *TetGen, a Delaunay-based quality tetrahedral mesh generator*. ACM Trans. Math. Softw. **41**, 11:1–11:36 (2015).
15. ICRP. *The 2007 recommendations of the international commission on radiological protection*. Ann. ICRP, ICRP publication 103 **37**, 1–332 (2007).
16. Yeom, Y. S., Jeong, J. H., Han, M. C. and Kim, C. H. *Tetrahedral-mesh-based computational human phantom for fast Monte Carlo dose calculations*. Phys. Med. Biol. **59**, 3173 (2014).
17. ICRP. *Nuclear decay data for Dosimetric calculations*. Ann. ICRP, ICRP Publication 107 **38** (2008).
18. Yeom, Y. S. *et al. Development of skeletal system for mesh-type ICRP reference adult phantoms*. Phys. Med. Biol. **61**, 7054 (2016).
19. ICRP. *Conversion coefficients for radiological protection quantities for external radiation exposures*. Ann. ICRP, ICRP Publication 116 **40**, 1–258 (2010).
20. Johnson, P. B., Bahadori, A. A., Eckerman, K. F., Lee, C. and Bolch, W. E. *Response functions for computing absorbed dose to skeletal tissues from photon irradiation—An update*. Phys. Med. Biol. **56**, 2347 (2011).
21. ICRP. *Basic anatomical and physiological data for use in radiological protection: Reference values*. Ann. ICRP, ICRP Publication 89 **32**, 1–277 (2002).
22. Lee, C., Kaufman, K., Pafundi, D. H. and Bolch, W. E. *An algorithm for lymphatic node placement in hybrid computational phantoms: applications to radionuclide therapy dosimetry*. Proc. IEEE **97**, 2098–2108 (2009).
23. ICRP. *Report on the task group on reference man*. Ann. ICRP/ICRP Publ. **23**, 1–480 (1975).
24. ICRP. *Human respiratory tract model for radiological protection: A report of a task Group of the International Commission on radiological protection*. Ann. ICRP, ICRP Publication 66 **23**, 1–482 (1994).